Image Fusion

Principles, Technology and Applications

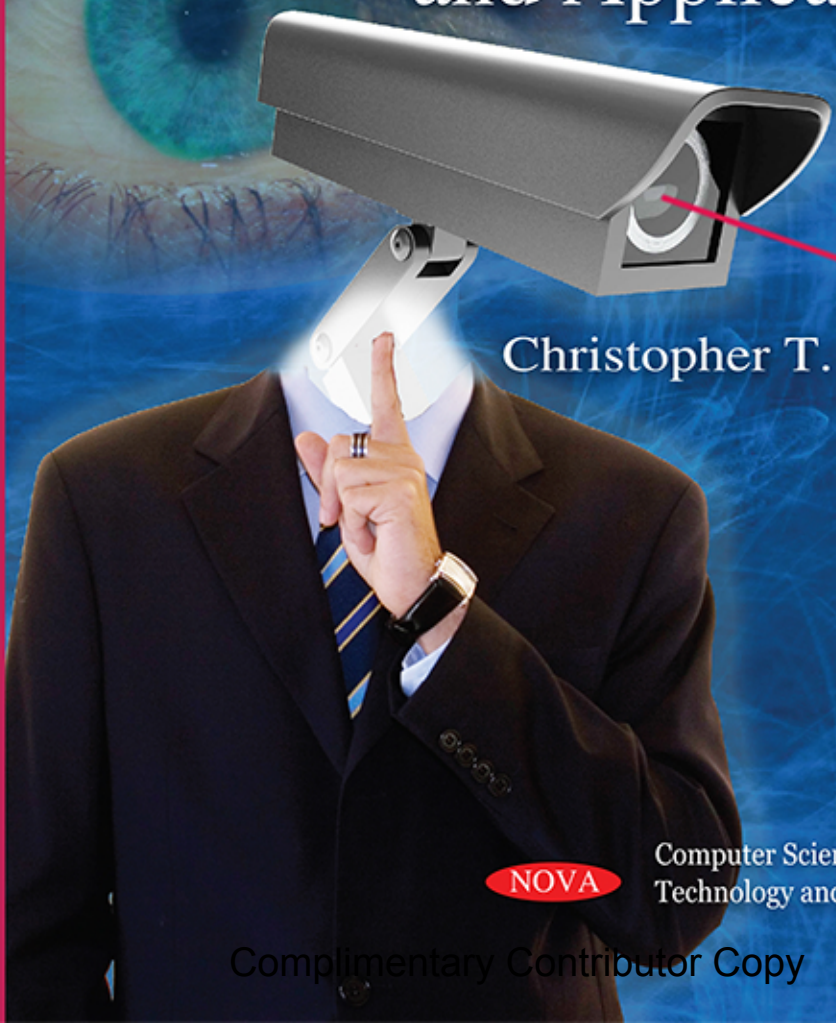

Christopher T. Davis
Editor

NOVA
Computer Science, Technology and Applications

COMPUTER SCIENCE, TECHNOLOGY AND APPLICATIONS

IMAGE FUSION

PRINCIPLES, TECHNOLOGY AND APPLICATIONS

CHRISTOPHER T. DAVIS
EDITOR

nova publishers
New York

In: Image Fusion
Editor: C. T. Davis, pp. 83-119
ISBN: 978-1-63482-115-5

Chapter 4

FUSION AND CLASSIFICATION OF MULTISOURCE IMAGES FOR UPDATE OF FOREST GIS

D. Amarsaikhan [*] ***and N. Ganchuluun***
Institute of Informatics and RS, Mongolian Academy of Sciences, Mongolia

Abstract

The main objectives of this chapter are to evaluate the performances of different image fusion techniques for the enhancement of spectral and textural variations of different forest types and toapply arefined maximum likelihood classifier for the extraction of forest class informationfrom the fused images in order to update a forest geographical information system (GIS). For the data fusion, modified intensity-hue-saturation (IHS) transformation, principal components analysis (PCA) method, Gram-Schmidt fusion, color normalization spectral sharpening, wavelet-based method, and Ehlers fusion are used and the results are compared. Of these methods, the better results are obtained through the use of the modifiedIHS transformation, PCA and wavelet-based fusion. The refined classification method uses spatial thresholds defined from contextual knowledge and different features obtained through a feature derivation process. The result of the refined classification is compared with the results of a standard method and it demonstrates a higher accuracy. Overall, the research indicates that multisource data fusion can significantly improve the interpretation and

[*] E-mail address: amar64@arvis.ac.mn (Corresponding author).

classification of forest types and the elaborated refined classification method is a powerful tool to increase classification accuracy.

Introduction

Forest is a very important natural resource that plays a significant role in keeping an environmental stability, ecological balance, environmental conservation, food security and sustainable development in both developed and developing countries[1]. In recent years, deforestation and forestland degradation have become the main concern for forest specialists and ecologists as well as policy and decision-makers dealing with the environment [2,3]. It has been found that much of the existing forests have been destroyed, mainly by shifting cultivation, timber preparation, legal and illegal logging, forest fires and increased number of people involved in agricultural activities [4,5,6,7]. To protect and conserve the deteriorating forest, it is vitally important for forest planners to have an updated forest map, integrate it with other thematic layers of a GIS and conduct sophisticated analysis.

In recent years, integrated approaches of optical and synthetic aperture radar (SAR) images have been increasingly used for forest mapping and analysis [8,9,10,11,12]. The combined application of optical and SAR data sets can provide unique information for different forest studies because passive sensor images will represent spectral variations of the top layer of the forest classes, whereas microwave data, with its penetrating capabilities, can provide some additional information about forest canopy. It is clear that the integrated use of the optical and microwave data sets can significantly improve forest class interpretation and analysis, because a specific forest type which is not seen on the passive sensor image may be observable on the microwave image and vice versa because of the complementary information provided by the two sources [13].

One of the prominent methods to combine remote sensing (RS) data from multiple sources is image fusion. Image fusion techniques usuallyattempt to combine images with different spectral and spatial resolutions and increase detailed information in the hybrid product produced by the fusion process [14,15,16]. Over the years, different fusion methods have been developed for improving spectral and spatial resolutionsof RS data sets. The techniques most encountered in the literature are the modified IHS transform, the Brovey transform, the PCA method, the Gram-Schmidt method, the local mean matching method, the local mean and variance matching method, the least square fusion method, the color normalization spectral sharpening, the wavelet-based fusion, the

multiplicative method and the Ehlers fusion [17,18,19]. Most image fusion applications use modified approaches or combinations of these methods.

Traditionally, multispectral RS data sets have been extensively used for forest mapping and, for this purpose, diverse classification methods have been applied. The traditional methods mainly involved supervised and unsupervised methods and hence, a great number of techniques have been developed [20]. Unlike single-source optical data, data sets from multiple sources have proved to offer better potential for discriminating between different forest cover types. Many authors have assessed the potential of multisource images for the classification of different forest classes [21,22,23,24,25]. In RS applications, the most widely used multisource classification techniques are parametric methods, neural networks, decision tree classifier, Dempster–Shafer theory of evidence, and knowledge-based methods [26].

The aims of this chapter are(a) to investigate and evaluate different image fusion techniques for the enhancement of spectral and textural variations of different forest types, later to be used for training sample selection, and (b) to apply arefined maximum likelihood classifier for the extraction of forest class informationfrom the fused images in order to update a forest GIS. The selected fusion techniques are themodifiedIHS transformation, the PCA method, the Gram-Schmidt fusion, the color normalization spectral sharpening, the wavelet-based method, and the Ehlers fusion. For the refined classification, spatial thresholds defined from the contextual knowledge were applied. For the analysis, optical and SAR images with different spatial resolutions as well as some GIS data of the forest area in Mongolia wereused.

Study Area and Data Sources

As a test site, Bogdkhan Mountain situated in central part of Mongolia, near the Ulaanbaatar city has been selected. It is a strictly protected area and one of the world's oldest officially and continuously protected sites. Officially declared a sacred mountain reserve in 1778, evidence of its protected status dates back to the 13th century. Because of its universal natural or cultural significance, the mountain was added to the UNESCO World Heritage Tentative List on August 6, 1996 [27].Within the vicinity of this region, the cutting of trees, polluting rivers, hunting of wild animals or digging of the land are severely prohibited.

The mountain has a territory of 41651ha, of which 55% is covered by forest. The entire massif extends about 32km from the East to the West and 16 km from the North to the South. It has 588 species of high plants, which are related to 256

genuses of 70 families. The 135 species such as carex, artemisa, oxytropis that relate to 11 main genuses comprise 22.9% of all species distributed on the mountain. Forest is distributed on the altitude range of 1400m (1450m)- 2100m (2150m) above sea level and consists of 3 sub zones such as mountain plateau, taiga and taiga type. Cedar and larch dominate the forest cover but pine, birch, spruce and poplar also occur [8].

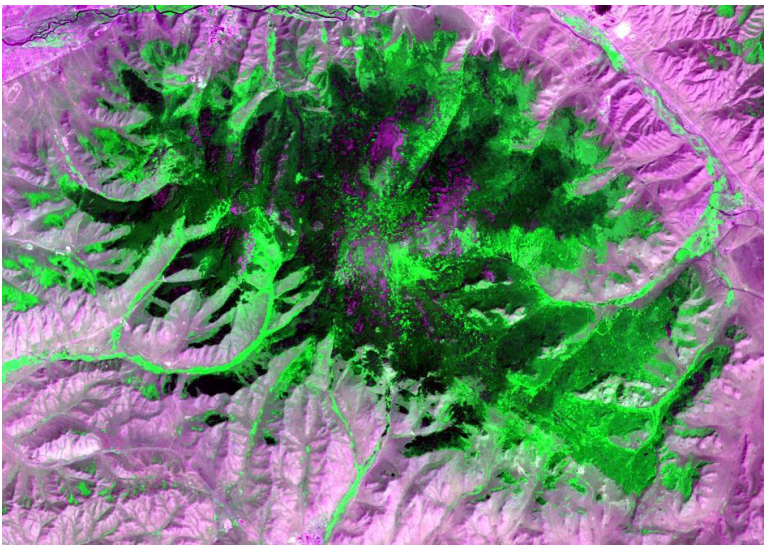

Figure 1. Landsat TM image of the Bogdkhan Mountain (R=band3, G=band4, B=band2). The size of the displayed area is about 28.2km x 20.0km.

The data used consisted of Landsat TM data from 31 July 2010 and Envisat SAR imageacquired on 25 March2010. The Landsat TM data have seven multispectral bands (B1: 0.45–0.52μm, B2: 0.52–0.60μm, B3: 0.63–0.69μm, B4: 0.76–0.90μm, B5: 1.55–1.75μm, B6: 10.40–12.50μm and B7: 2.08–2.35μm). The spatial resolution is 30 m for the reflective bands, while it is 120 m for the thermal band. In the current study, channels 2,3,4,5 and 7 have been used. The Envisat is a European Earth-observing satellite carrying a cloud-piercing, all-weather free polarimetric radar, which is designed to monitor the Earth from a distance of about 790km. In the present study, a C-band (i.e.5.36GHz) HH polarization image has been selected. In addition, a topographic map from 1969, scale 1:50,000 and a forest taxonomy map (made by the combined use of an aerial photograph from 1963 and ground survey from 1988), scale 1:100,000 were available, accordingly.

Figure 1 shows the study area in a Landsat TM image of 2010 and some examples of its forest cover.

Georeferencing of Multisource Images

In order to perform accurate data fusion, both high geometric accuracy and good geometric correlation between the images are needed. Initially, the Envisat image was rectified to the coordinates of the Landsat TMimage using 11 more regularly distributed ground control points (GCP)s defined from topographic and forest taxonomy maps of the study area. The GCPs have been selected on clearly delineated sites such as morphological structures, forest areas and roads. For the transformation, a second-order transformation and nearest-neighbour resampling approach were applied and the related root mean square (RMS) error was 0.526 pixels. The original and predicted coordinates as well as error values in both x and y directions are shown in Table 1. As seen from the Table 1, for each of the selected GCP, the RMS error is lower than 0.9 pixels. It indicates that there is a good geometric correspondence between the two images.

Table 1. The selected GCPs and total RMS error

No	Base X	Base Y	Warp X	Warp Y	Predict X	Predict Y	Error X	Error Y	RMS
1	4985.25	2652.75	2304.50	2068.50	2304.52	2068.51	0.021	0.011	0.0239
2	4046.00	1846.75	843.00	1151.00	842.82	1151.34	-0.174	0.349	0.3904
3	4070.50	1974.75	899.75	1320.25	899.43	1319.78	-0.313	-0.462	0.5584
4	4195.00	2472.25	1188.00	1978.00	1187.91	1977.95	-0.089	-0.041	0.0986
5	4660.00	1928.00	1704.00	1144.00	1704.02	1143.90	0.020	-0.091	0.0941
6	4535.25	2756.00	1706.00	2300.00	1705.99	2299.98	-0.007	-0.014	0.0168
7	4902.00	2348.00	2136.00	1669.00	2135.81	1668.88	-0.182	-0.115	0.2155
8	3888.00	2139.50	684.00	1584.00	684.20	1584.14	0.200	0.144	0.2474
9	4210.00	1790.50	1056.75	1042.00	1057.65	1041.27	0.900	-0.728	1.1582
10	4277.00	1799.00	1151.25	1038.75	1150.56	1039.45	-0.682	0.708	0.9840
11	4668.50	2288.75	1795.00	1630.75	1795.30	1630.98	0.302	0.235	0.3836

Total RMS Error: 0.526.

After the first co-registration of the coordinates, the combined Envisat SAR and Landsat TM images have been georeferenced to a UTM map projection using the topographic map of the study area. For the projection parameters, Zone 48N and WGS84 Datum were used. The GCPs have been selected on clearly delineated sites and, in total, 9 randomly distributed points were chosen. For the actual transformation, a second-order transformation was used. As a resampling

technique, the nearest-neighbour resampling method was applied and the related RMS error was 0.35 pixels.

Speckle Suppression of the SAR Image and Derivation of the Texture Features

As the microwave images have a granular appearance, due to the speckle formed as a result of the coherent radiation used for radar systems, the reduction of the speckle is a very important step in further analysis. The analysis of the radar images must be based on the techniques that remove the speckle effects while considering the intrinsic texture of the image frame [28,29]. In this study, five different Speckle suppression techniques such as lee, local region, frost, kuan and gammamap filters [30] of 3x3 and 5x5 sizes were compared in terms of delineation of forested areas and texture information. After visual inspection of each image, it was found that the 3x3 gammamap filter created the best image in terms of delineation of different features as well as preserving content of texture information. In the output image, speckle noise was reduced with very low degradation of the textural information. Comparison of the selected and other SAR images is shown in figure 2.

In RS image analysis, texture is usually applicable to radar data. The ability to use radar data to detect texture and provide topographic information is a major advantage over other types of imagery [30]. To derive texture images, occurrence and co-occurrence measures (using 9x9 and 11x11 window sizes) were applied to the SAR image. The occurrence measures use the number of occurrences of each grey level within the processing window for the texture calculations, while the co-occurrence measures use a grey-tone spatial dependence matrix to calculate texture values [31]. By applying these measures, initially 20 features have been obtained, but after thorough checking of each individual feature, only 3features including the resultsof11x11 skewness, 9x9 contrast and 9x9 correlation filters were selected.

The skewness can be mathematically defined as the averaged cubed deviation from the mean divided by the standard deviation cubed. The contrast measure indicates how most elements do not lie on the main diagonal, whereas, the correlation measure is used to compare the similarity of two input signals as they are shifted by one another. The texture features can be used in several ways to increase the use of a SAR image. For example, adding the texturally enhanced radar image as an additional feature to the original data set should be useful for increasing the accuracy in a forest classification. Figure 3 shows the results of the

skewness, contrast and correlation filters combined in a RGB (red, green and blue) domain.

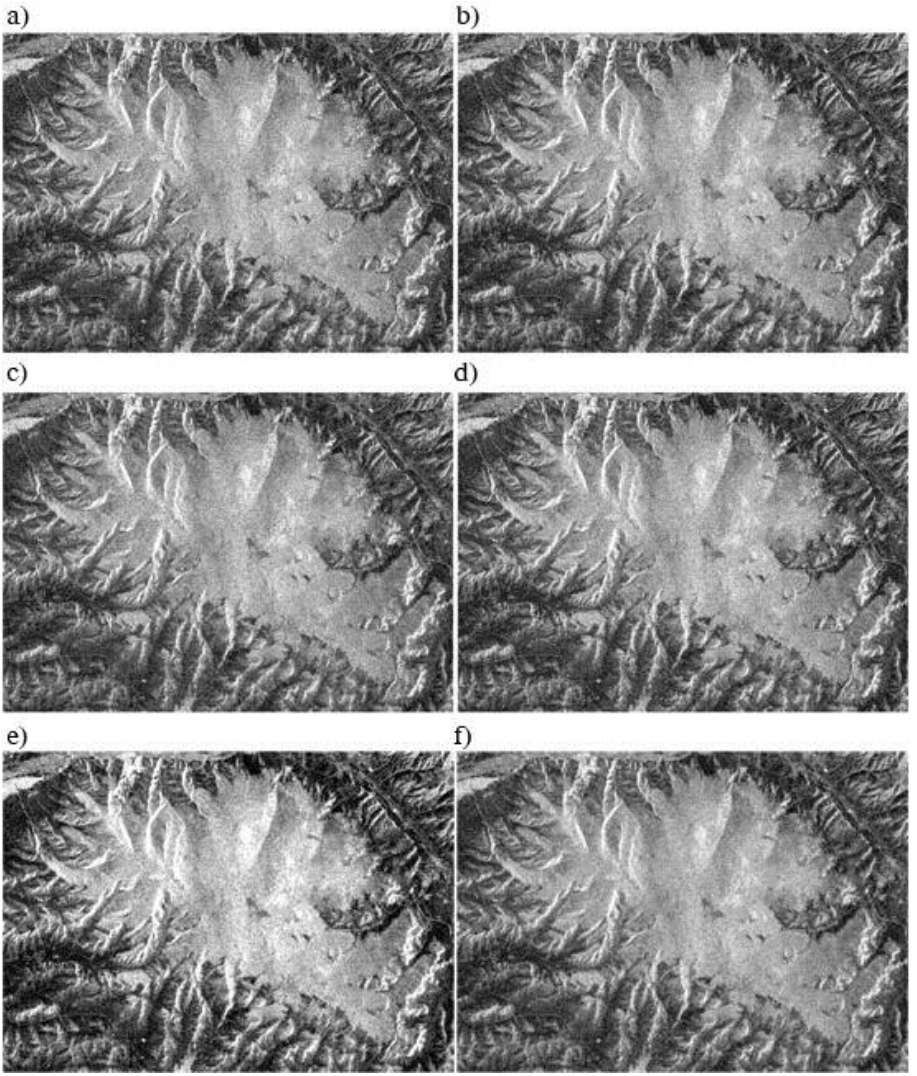

Figure 2. Comparison of the SAR images: (a) the original SAR image; (b) the image obtained by a 3x3 lee filter;(c) the image obtained by a 3x3 local region filter; (d) the image obtained by a 3x3 frost filter; (e) the image obtained by a 3x3 kuan filter; and (f) the image obtained by a 3x3 gammamap filter.

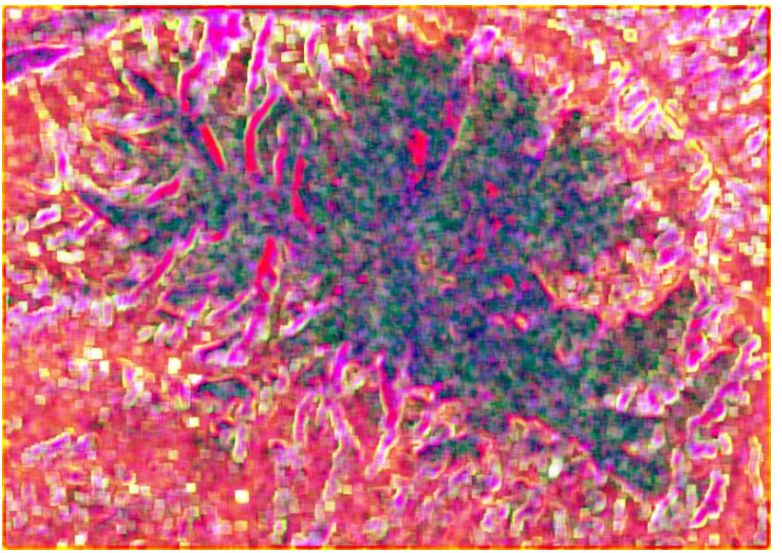

Figure 3. A colour image created by the texture filters (R=result of the contrast filter. G=result of the correlation filter, B=result of the skewness filter).

Image Fusion Methods

The image fusion refers to a process that integrates different images from different sources to obtain more information, considering a minimum loss or distortion of the original data. In other words, the image fusion is the integration of different digital images in order to create a new image and obtain more information than can be derived separately from any of them [16,32,33]. In the case of the present study, the SAR image provides some information about forest canopy due to radar's penetrating capabilities, while the TM image provides the information about the spectral variations of different forest classes. Over the years, different data fusion techniques have been developed and applied, individually and in combination, providing users and decision-makers with various levels of information. Generally, image fusion can be performed at four different stages: signal level, pixel level, feature level, and decision level [34]. In this study, data fusion has been performed at a pixel level and the following techniques were compared: (a) modifiedIHS transformation, (b) PCA method, (c) Gram-Schmidt fusion, (d) color normalization spectral sharpening, (e) wavelet-based method, (f) Ehlers fusion. Each of these techniques is briefly discussed below.

Modified IHS transformation: This method has a vast improvement over the traditional IHS for fusing satellite imagery; differing noticeably in spectral response. It allows combination of single-band panchromatic data with multispectral data, resulting in an output with both excellent detail and a realistic representation of original multispectral scene colors. In general, the HIS transformation separates spatial (intensity) and spectral (hue and saturation) information from a standard RGB image. The intensity refers to the total brightness of the image, hue to the dominant or average wavelength of the light contributing to the color and saturation to the purity of color. To fuse the images, three bands of a multichannel image are transformed from the RGB domain into the IHS color space. The panchromatic component is matched to the intensity of the IHS image and then replaces the intensity component. The modified IHS method is designed to produce an output that approximates the spectral characteristics of the input multispectral bands while preserving the spatial integrity of the panchromatic data. The technique works by assessing the spectral overlap between each multispectral band and the high resolution panchromatic band and weighting the merge based on these relative wavelengths [35].

PCA method: In RS image analysis, the PCA is usually considered as a data compression technique used to reduce the dimensionality of the multiband datasets [36]. It is also helpful for image encoding, enhancement, change detection and multitemporal dimensionality [32]. When the PCA is performed, the axes of the spectral space are rotated, changing the coordinates of each pixel in spectral space. The new axes are parallel to the axes of the ellipse. The length and direction of the widest transect of the ellipse are calculated using a matrix algebra. The transect, which corresponds to the major axis of the ellipse, is called the first principal component of the data. The direction of the first principal component is the first eigenvector, and its length is the first eigenvalue. A new axis of the spectral space is defined by this first principal component. The second principal component is the widest transect of the ellipse that is perpendicular to the first principal component. As such, the second principal component describes the largest amount of variance in the data that is not already described by the first principal component. In n dimensions, there are n principal components. Each successive principal component is the widest transect of the ellipse that is orthogonal to the previous components in the n-dimensional space and accounts for a decreasing amount of the variation in the data which is not already accounted for by previous principal components [30].

Gram-Schmidt fusion: This fusion technique transforms a set of multidimensional features into a new set of orthogonal and linear independent features. By averaging the multispectral bands, the method simulates a low resolution panchromatic band. As the next step, theGram-Schmidt transform is performed for the simulated panchromatic band and the multispectral bands with the simulated panchromatic band applied as the first band. Then the high spatial resolution panchromatic band replaces the first component [37]. Finally, an inverse transform is applied to create the spatially and spectrally enhanced multispectral bands.

Color normalization spectral sharpening: This is an extension of the color normalized algorithm. The input image bands are grouped into spectral segments defined by the spectral range of the panchromatic image. The corresponding band segments are processed in the manner that each input band is multiplied by the sharpening band and then normalized by dividing it by the sum of the input bands in the segment. Bands outside the spectral range of the panchromatic image are not sharpened [38]. Unlike many other sharpening techniques, this method can be used to simultaneously sharpen any number of bands and retain the input image's original data type and dynamic range.

Wavelet-based fusion: The wavelet transform decomposes the signal based on elementary functions, that is, the wavelets. By using this, an image is decomposed into a set of multi-resolution images with wavelet coefficients. For each level, the coefficients contain spatial differences between two successive resolution levels. In general, a wavelet-based image fusion can be performed either by replacing some wavelet coefficients of the low-resolution image with the corresponding coefficients of the high-resolution image or by adding high-resolution coefficients to the low-resolution data [39]. In the current study, the first approach, which is based on bi-orthogonal transforms, has been applied.

Ehlers fusion: This method is based on an IHS transform coupled with a Fourier domain filtering and it is extended to include more than 3 bands by using multiple IHS transforms until the number of bands is exhausted. A subsequent Fourier transform of the intensity component and the panchromatic image allows an adaptive filter design in the frequency domain. Using fast Fourier transform techniques, enhancement or suppression of the spatial components can be directly accessed. The intensity spectrum is filtered with a low pass filter whereas the panchromatic spectrum is filtered with an inverse high pass filter. After filtering, the images are transformed back into the spatial domain with an inverse fast Fourier transform and added together to form a fused intensity component with the low-frequency information from the low resolution multispectral image and the high-frequency information from the high resolution image. This new intensity

component, the original hue, and the saturation components of the multispectral image form a new IHS image. As the last step, an inverse IHS transformation produces a fused RGB image. These steps can be repeated with successive 3-band selections until all bands are fused with the panchromatic band [40].

Interpretation and Comparison of the Fused Images

Initially, the aforementioned fusion techniques have been applied to the combined Landsat TM, Envisat SAR and texture images. In all cases, the SAR image was considered as a high resolution band. In order to obtain good colour images that can illustrate spectral and spatial variations of the available forest classes on the selected multisource image, all the fused images have been visually inspected and compared.

Table 2. Principal component coefficients from TM, SAR and texture images

Bands	PC1	PC2	PC3	PC4	PC5	PC6	PC7	PC8	PC9
TM2	0.091	-0.071	0.129	0.001	0.081	-0.001	-0.464	0.305	0.808
TM3	0.162	-0.12	0.222	-0.001	0.230	0.008	-0.675	0.263	-0.575
TM4	0.040	-0.038	0.100	0.023	-0.914	-0.001	-0.319	-0.218	-0.032
TM5	0.417	-0.285	0.576	0.025	-0.162	0.083	0.467	0.398	-0.030
TM7	0.282	-0.196	0.385	0.006	0.276	0.077	-0.081	-0.794	0.114
SAR	-0.799	-0.015	0.579	0.123	0.027	-0.097	0.010	0.001	-0.001
Contrast_F	-0.228	-0.915	-0.303	-0.109	-0.010	0.076	0.007	0.001	-0.001
Correlation_F	0.118	-0.107	0.002	-0.042	0.007	-0.985	0.0284	-0.027	0.001
Skewness_F	0.066	-0.095	-0.126	0.984	0.019	-0.024	-0.003	-0.001	-0.001
Eigenvalues	3392.8	2520.2	895.3	208.7	100.1	72.3	23.3	3.7	0.6
Variance (%)	47.00	34.92	12.40	2.89	1.38	1.00	0.32	0.08	0.01

In the case of the modifiedIHS transformation method, the fused image (Figure 4a) demonstrated a better result compared to some other combinations, because beside the improved textural enhancement, the image has good spectral separations among some coniferous and deciduous forests. However, on the image it was not easy to perceive the separations between spruce and cedar forests.

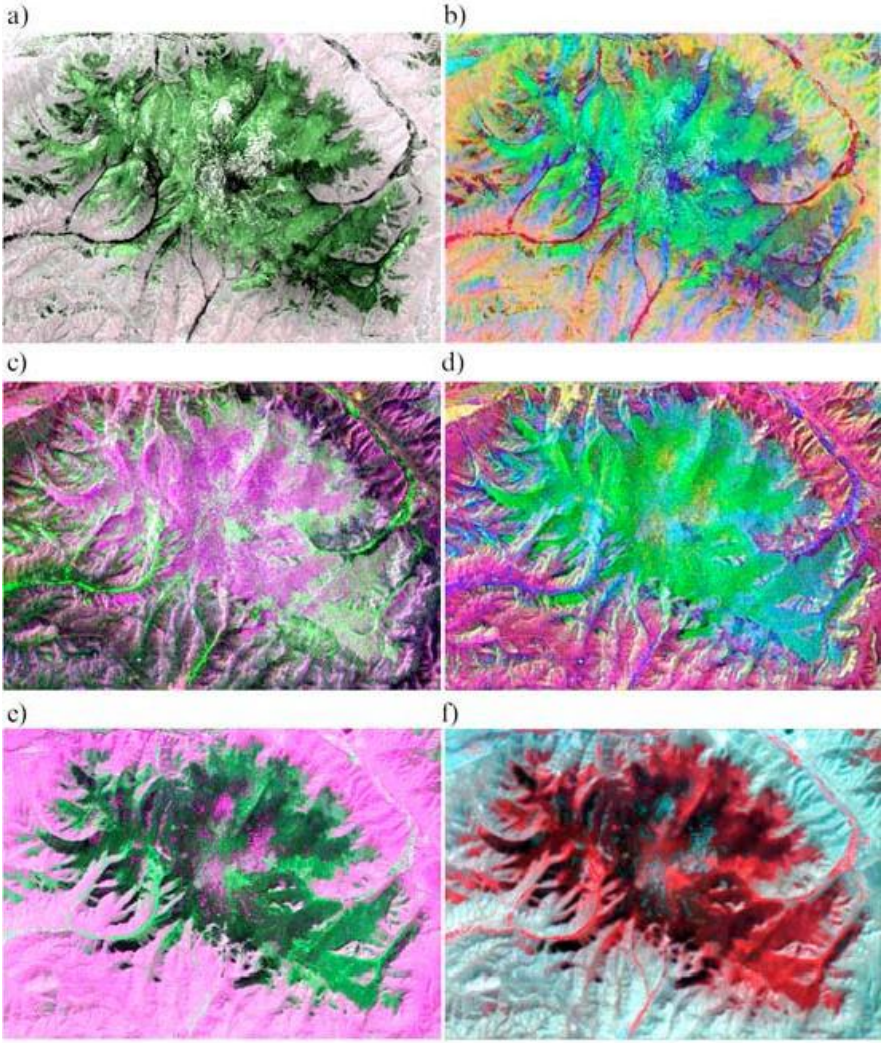

Figure 4. Comparison of the fused multisource images: (a) the image obtained by modified IHS transformation; (b) the PC image (red=PC1, green=PC3; blue=PC5); (c) the image obtained by Gram-Schmidt fusion; (d) the image obtained bycolor normalization spectral sharpening; (e)the image obtained by wavelet-based method; and(f) the image obtained by Elhers fusion.

PCA has been applied to all selected images and the result of the final analysis is shown in table 2. As can be seen from table 2, the Envisat HH polarisation image has a high negative loading in PC1 which contains 47% of the

overall variance. This means that the PC1 is dominated by the characteristics of the SAR image. Although, PC2 contained 34.92% of the overall variance and had a very high negative loading of the result of the contrast filter, visual inspection revealed that it contained less information related to the available forest classes. In PC3 that contains 12.4% of the overall variance, the middle infrared band of TM and SAR image have moderately high loadings. Compared to the PC2, on this image, it was possible to see some tonal variations of different forest classes. It was seen that the PC4 dominated by the result of theskewness filter had no useful information. However, visual inspection of PC5 that contained only 1.38 % of the overall variance, in which near infrared band of TM had a very high negative loading, revealed that this feature contained useful information related to the tonal variations as well as textural characteristics of different forest classes. The PC6 and PC7 dominated by the negative characteristics of thecorrelation filter and visible bands had some useful information. The inspection of the remaining PCs indicated that they contained noise from the total data set. The PC image created by the combinations of PC1, PC3 and PC5 is shown in figure 4b. As seen from the PC image, though the image cannot show clear textural features, it could well illustrate the colour variations of different classes, specifically among larch, cedar, birch and spruce forests.

In the cases of the Gram-Schmidt fusion and color normalization spectral sharpening, the results are worse than the images created by other fusion techniques. As seen from the results shown in Figure 4c,d, these images are dominated by the characteristics of the SAR image. It is possible to observe only some separations of the larch forest, and other forest types are almost not distinguishable on these images. In the case of the wavelet-based fusion, the integrated image (Figure 4e) demonstrated a better result compared to the results of the Gram-Schmidt fusion and color normalization spectral sharpening. On this image, larch, cedar, pine and spruce forest types could be distinguished by their spectral properties. Additionally, it could be seen that the image illustrates good textural differentiation between different forest types. In the case of the Ehlers fusion, the fused image (Figure 3f) demonstrated a better result compared to some other combinations, but it had a blurred appearance due to speckle noise. However, on this image it is possible to observe some spectral separations among larch, cedar, spruce and pine forests. Figure 4 shows the comparison of the images obtained by the selected fusion methods.

Evaluation of Features and Standard Classification

At the beginning, in order to define the sites for the training signature selection, from the multisensor images, several areas of interest (AOI)s representing the selected forest classes (i.e., larch, cedar, pine, birch and spruce) have been selected through thorough analysis using a polygon-based approach. For the selection of the sites of training samples, the images obtained by the modifiedIHS transformation, PCA and wavelet-based method have been compared. The separability of the training signatures was first checked in feature space. If the signatures are overlapped in feature space, then they are not separable (Figure 5a). If they are separable, there is no overlap between the signatures (Figure 5b). After checking the signatures in feature space, they were evaluated using Jeffries–Matusita distance. The values of Jeffries–Matusita distance range from 0 to 2.0 and indicate how well the selected pairs are statistically separate. The values greater than 1.9 indicate that the pairs have good separability [30]. After the investigation, the samples that demonstrated the greatest separability were chosen to form the final signatures. The final signatures included 3923 pixels for larch forest, 2535 pixels for cedar forest, 124 pixels for pine forest, 802 pixels for spruce forest and 320 pixels for birch forest. As seen from the separabilities measured by Jeffries–Matusita distance (Table 3), the available forest classes have high statistical overlaps.

Table 3. The separabilities measured by Jeffries–Matusita distance

	Birch	**Larch**	**Pine**	**Spruce**	**Cedar**
Birch	0.000	1.600	1.856	1.980	1.975
Larch	1.600	0.000	1.594	1.698	1.697
Pine	1.856	1.594	0.000	1.446	1.507
Spruce	1.980	1.698	1.446	0.000	1.235
Cedar	1.975	1.697	1.507	1.235	0.000

In many cases, forest types have similar spectral characteristics and it is not easy to separate them by the use of ordinary feature combinations or fusing techniques. For the successful extraction of the forest classes, reliable features derived from multiple sources should be used. In the case of the present study, texture features might be considered as additional sources. For the classification, the following feature combinations were used:

The original five spectral bands of the Landsat TM data.
The green, red, near infrared and middle infrared (2-5) bands of the Landsat TM data.
The HH polarization component of Envisat SAR and original five spectral bands of the Landsat TM data.
The PC1, PC2 and PC3 of the PCA.
The PC1, PC2, PC3, PC4 and PC5 of the PCA.
The PC1, PC2, PC3, PC4, PC5, PC6 and PC7 of the PCA.
Multiple bands including the original Envisat SAR and Landsat TM data as well as three texture images.
Fuzzy convolution applied to the classification result of the multiple bands that include the original SAR, Landsat TM and three texture images.

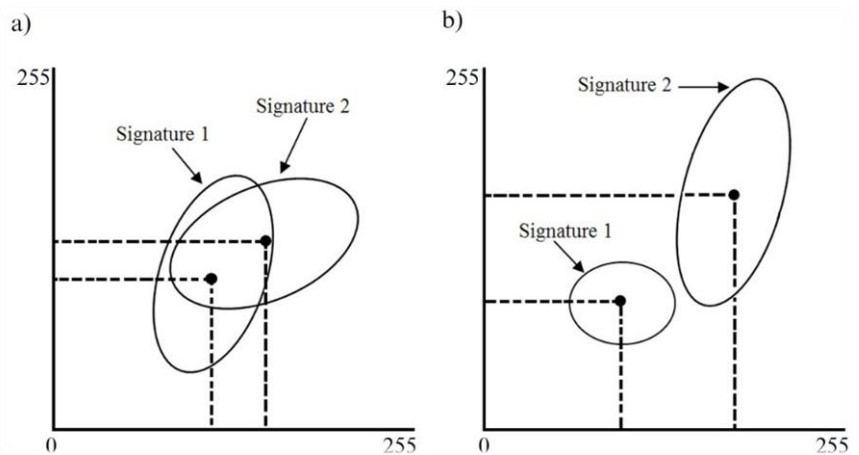

Figure 5. Comparison of the overlapped (a) and unoverlapped (b) signatures.

For the actual classification, a supervised statistical maximum likelihood classification (MLC) has been used assuming that the training samples have the Gaussian distribution. The basis of a maximum likelihood classification (MLC) are the actual frequencies of co-occurrence ($Freq(C_i,x)$) between class (C_i) and an observation vector (x). In the case of multidimensional RS data, we assume that each observation x (pixel) consists of a set of measurements on N variables (features) [28]. The decision rule, assuming Bayes' rule, can be written as follows:

$$P(C_i|x) = P(x|C_i) \bullet P(C_i)/P(x) \quad (1)$$

$P(x|C_i)$ is approximated by a multivariate normal probability density function and it is scaled by a priori probability ($P(C_i)$). This function has as parameters a mean vector (m_i) and covariance matrix (Σ_i) for each class (C_i). These parameters have to be estimated on the basis of a training set or clusters. The formula for the approximation is expressed as follows:

$$P(X|Ci) = (2\pi)^{-\frac{N}{2}} \left|\sum_i\right|^{-\frac{1}{2}} \exp\{-\frac{1}{2}(x-m_i)^t \sum_i^{-1}(x-m_i)\} \tag{2}$$

$P(C_i)$ is defined by the user's prior knowledge about the area.

$P(x)$ is the probability of finding a pixel from any class and expressed as:

$$P(x) = \sum_{i=1}^{n} P(x \mid Ci) \bullet P(Ci) \tag{3}$$

The actual classification is performed according to $P(C_i|x) > P(C_j|x)$ for all $j \neq i$.

However, $P(x)$ is common to all classes and is usually dropped from the actual classification. In this case, for the classification, the following discriminant function is used:

$$g_i(x) = Ln\{P(x|Ci)\} + Ln\{P(Ci)\} \tag{4}$$

In many cases, the users assume that the classes have equal prior probabilities. In this case, $P(C_i)$ can also be dropped and the discriminant function can be written as follows:

$$g_i(x) = Ln\{P(x|Ci)\} \tag{5}$$

and the classification is performed according to $g_i(x)>g_j(x)$ for all $j \neq i$.

The rule has the maximum benefit of correct classification; that is,a pixel classified by this method has the maximum probability of correct assignment. Therefore, the method is considered as one of the most efficient methods for statistical pattern recognition [41].

For the accuracy assessment, the overall performance has been used. This approach creates a confusion matrix in which reference pixels are compared with the classified pixels and as a result an accuracy report is generated indicating the percentages of the overall accuracy [42]. Forground truth information, different

regions containing purest pixels have been selected. The regions were selected on a principle that there were more available pixels to be selected for the evaluation of the larger classes, such as larch and cedar forests, than the smaller classes such as pine and birch forests.

Classification Result Using Original Five Spectral Bands

The MLC of the Bogdkhan Mountain has been performed using the original five spectral bands of the Landsat TM data.

Table 4. The overall classification accuracy of the classified image

	Birch	Larch	Pine	Spruce	Cedar
Birch	201	813	2	0	2
Larch	16	4328	17	26	42
Pine	8	573	52	33	112
Spruce	0	147	2	594	246
Cedar	0	38	51	146	2122

Overall Accuracy = (7297/9571) 76.24%.

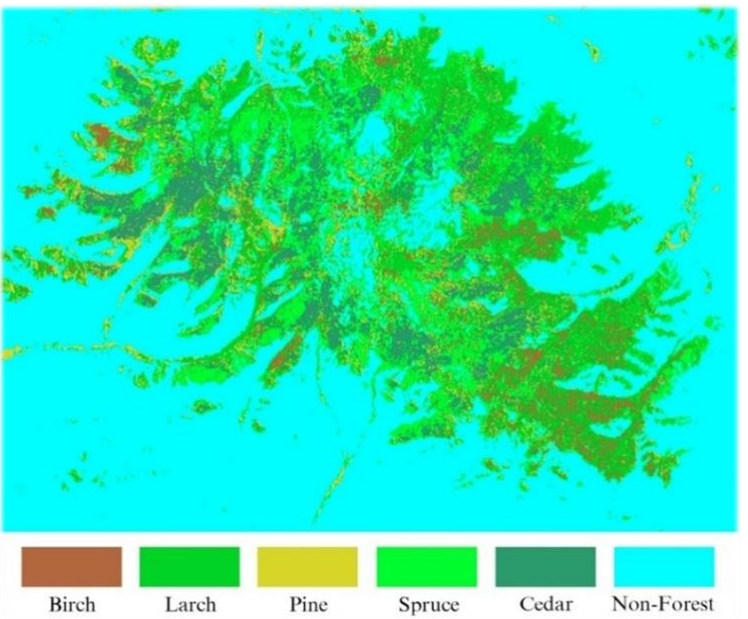

Figure 6. Classification result using original five spectral bands.

The decision-rule used the signatures defined from the signature evaluation process (i.e., 3923 pixels for larch forest, 2535 pixels for cedar forest, 124 pixels for pine forest, 802 pixels for spruce forest and 320 pixels for birch forest) and assumed that the selected classes have equal prior probabilities. The final classified image is shown in Figure 6. The overall classification accuracy for the selected classes is shown in Table 4. Asseen from the classification result, the accuracy of the MLC is not high (i.e., 76.24%) and there are high mixtures among birch, larch, cedar and spruce forests.

Classification Result Using Green, Red, Near Infrared and First Middle Infrared Bands

The classification of the test area has been made using the green, red, near infrared and first middle infrared bands of the Landsat TM data. The decision-rule used the same signatures defined from the signature evaluation process and the same assumption of equal prior probabilities. The final classified image is shown in Figure 7. As seen from the classified image, the result is very similar to the result obtained by the use of the original five spectral bands.

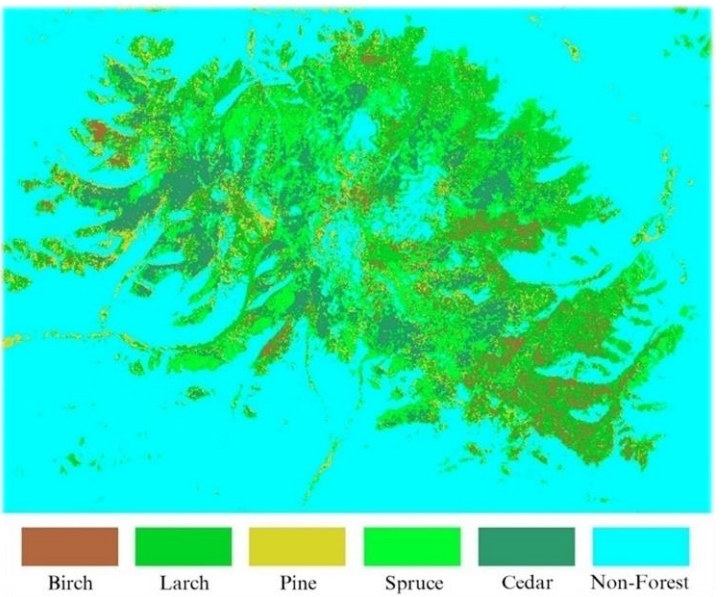

Figure 7. Classification result using four spectral bands.

Table 5. The overall classification accuracy of the classified image

	Birch	Larch	Pine	Spruce	Cedar
Birch	200	811	4	0	3
Larch	15	4335	14	30	46
Pine	10	563	49	31	49
Spruce	0	163	3	592	252
Cedar	0	30	54	145	2177

Overall accuracy = (7353/9576)76.78%.

The overall classification accuracy for the selected five forest classes is shown in Table 5. It has been evaluated using the same set of regions containing the purest pixels as in the previous classification, and it demonstrated an overall accuracy of 76.78%.As could be seen from the confusion matrix shown in Table 5, the performance of the MLC is better than the previous case and it has a tiny improvement. In many cases, users and analysts expect that the addition of more spectral bands would increase the classification accuracy. However, the current study indicates that it is not always true. This is due to a fact that the inclusion of more bands may result in a signature overlap in multidimensional feature space. Therefore, in some cases it is desirable to select a few less-correlated bands.

Classification Result Using SAR and Original Five Spectral Bands

The MLC of the test site has been performed using the HH polarization component of Envisat SAR and original five spectral bands of the Landsat TM data.

Table 6. The overall classification accuracy of the classified image

	Birch	Larch	Pine	Spruce	Cedar
Birch	206	762	2	0	2
Larch	11	4413	6	23	59
Pine	7	551	79	29	127
Spruce	0	134	5	564	179
Cedar	1	48	32	184	2163

Overall Accuracy = (7425/9587) 77.45%.

The result of the classification is shown in Figure 8. As seen from the classified image, the result looks similar to the results obtained by the use of original Landsat TM bands. However, the confusion matrix (Table 6) indicated an

overall accuracy of 77.45%. This means that the combined use of optical and microwave data sets produced a better result than the single source image, but the result is still insufficient.

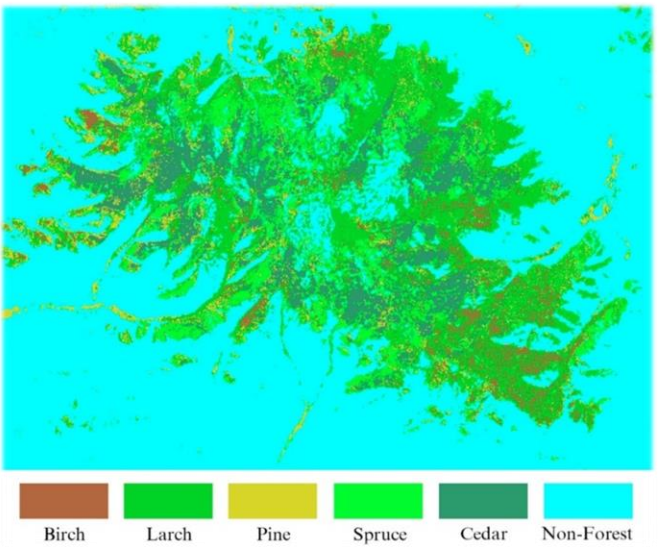

Figure 8. Classification result using SAR and five spectral bands.

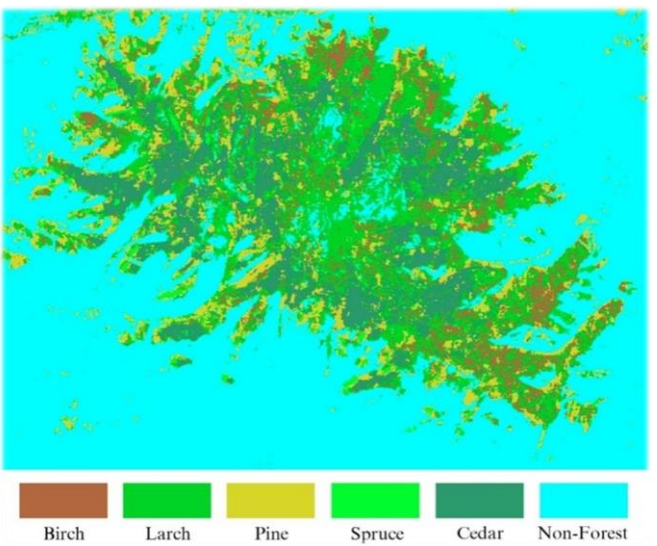

Figure 9. Classification result using the first three PCs.

Classification Result Using the First Three PCs

As it was seen from Table 2, the PC1, PC2 and PC3 of the PCA included 94.32% of the overall variance.

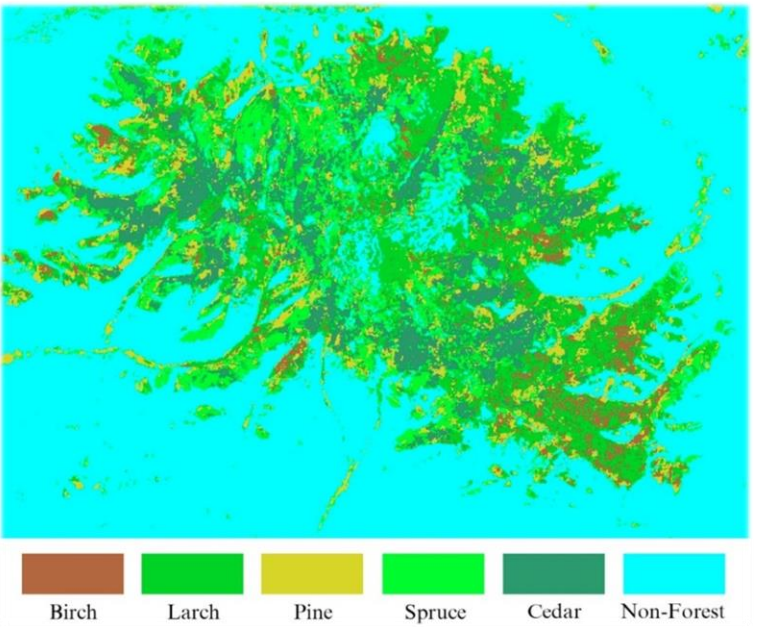

Figure 10. Classification result using the first five PCs.

Table 7. The overall classification accuracy of the classified image

	Birch	Larch	Pine	Spruce	Cedar
Birch	183	2053	13	32	7
Larch	26	3145	15	51	74
Pine	11	480	51	116	67
Spruce	4	104	9	162	100
Cedar	1	114	36	433	2286

Overall Accuracy = (5827/9573) 60.86%.

In many PC-based image analysis, the selection of the first three PCs may be sufficient, if their overall variance exceeds 95%. In the case of the present study, as the overall variance almost reached that level, the PC1, PC2 and PC3 were classified using the MLC. Figure 9 shows the result of the classification and Table

7 indicates the overall accuracy. As seen from the results, the MLC of the first three PCs gives the worst result, because there are different mixtures among all classes. Specifically, there are high mixtures among the birch, larch and spruce forests. Also, many pixels belonging to the pine forest have been misclassified. This indicates that it is not necessary for the first three PCs to produce an improved classification result.

Table 8. The overall classification accuracy of the classified image

	Birch	Larch	Pine	Spruce	Cedar
Birch	204	1013	6	2	2
Larch	17	4133	15	29	42
Pine	1	546	66	17	135
Spruce	0	173	4	540	162
Cedar	3	46	33	211	2191

Overall Accuracy =(7134/9591) 74.38%.

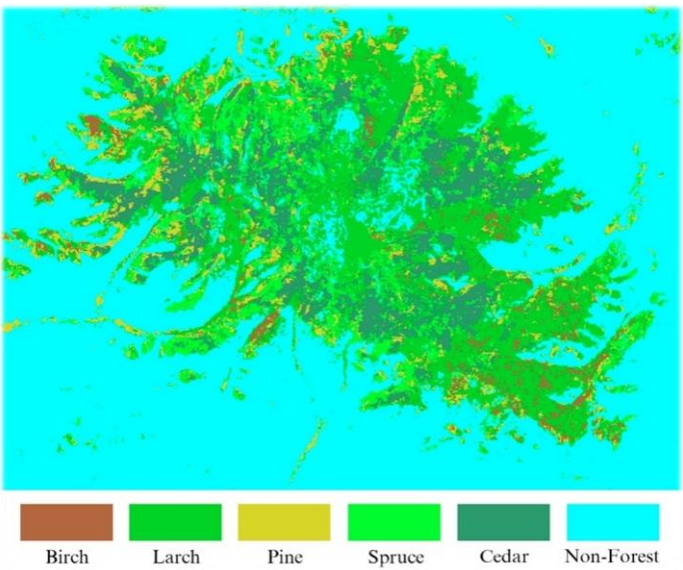

Figure 11. Classification result using the first seven PCs.

Classification Result Using the First FivePCs

As could be seen from Table 2, thePC1, PC2, PC3, PC4 and PC5 of the PCA included 98.59% of the overall variance. The result of the classification is shown in Figure 10 and the overall accuracy is illustrated in Table 8. As seen from the results, there is a significant improvement in the classification performance. For example, there are reduced mixtures among the forest classes compared to the case of the first three PCs. The PCA indicated that there was addition of only 4.27% in the overall variance, but the substantial improvement occurred in the classification accuracy.

Classification Result Using the First Seven PCs

As could be seen from Table 2, the first seven PCs included 99.91%of the overall variance (i.e., it exceeds the overall variance of the first five PCs by only 1.32%).

Table 9. The overall classification accuracy of the classified image

	Birch	Larch	Pine	Spruce	Cedar
Birch	206	488	1	0	0
Larch	17	4708	6	30	54
Pine	0	489	89	20	208
Spruce	0	179	3	563	128
Cedar	2	44	25	186	2143

Overall Accuracy = (7709/9589)80.39%.

The chosen PCs have been classified using the MLC and the result is shown in Figure 11. The confusion matrix (Table 9) indicated an overall accuracy of 80.39%, indicating an improvement occurred in the classification performance compared to the previously classified PC images. As could be seen from the PCA, the first five PCs weredominated by different characteristics of the near infrared, middle infrared, SAR and two texture features and their classification accuracy was not high enough. This was due to a fact that these bands composed of different features with a variety of different characteristics could not create orthogonal features in a multidimensional feature space. When the PC6 and PC7, dominated by the negative characteristics of the correlation filter and visible bands of the Landsat TM, have been added to the first five PCs, the overall classification accuracy was increased by 6.01%. This means that some useful information might be included in the last PCs that contain a negligible part of the

overall variance. In the present study, due to the addition of the PC6 and PC7 (i.e., the overall variance has been increased by only 1.32%), the classification accuracy was increased from 74.38% to 80.39%.

Classification Result Using Original SAR, Landsat TM and Three Texture Images

In most cases, for the successful classification of the statistically overlapping classes, reliable additionalfeatures derived from multiple sources should be used in a decision-making process. In the current study, the texture images derived from the original SAR band, could be considered such additional features. The classification of the Bogdkhan Mountain has been performed using all 9 bands. The result of the MLC is shown in Figure 12 and the overallclassification accuracy is illustrated in Table 10.

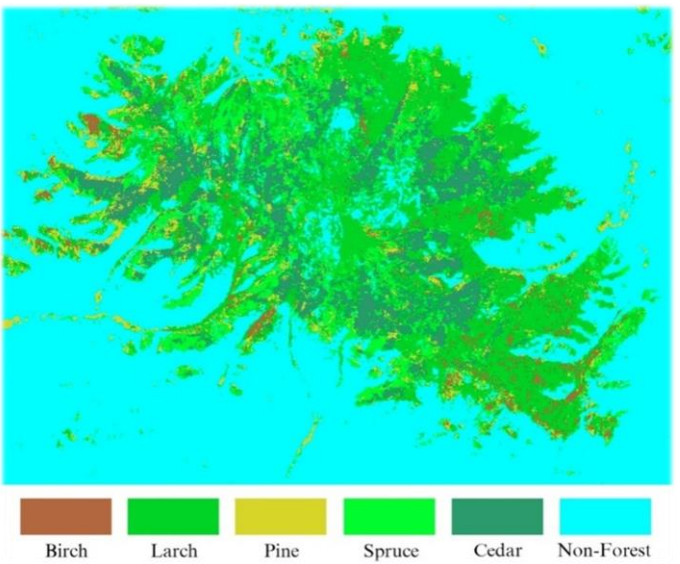

Figure 12. Classification result using multiple bands.

The classification results indicated that some improvements occurred in the overall accuracy of the MLC compared to the classification result of the first seven PCs. For example, in the case of the first seven PCs (Table 9), 488 pixels belonging to the larch forest and 208 pixels of the cedar forest have been classified as birch and pine forests, while in the classification of multiple bands

(Table 10) 352 and 154 pixels of the same forest classes were misclassified as the birch and pine forests. Likewise, 489 pixels of the larch forest of the classified PC image have been misclassified as pine forest, whereas 275 pixels of the same class were classified as the pine forest.

As seen from the comparison of the classified images, the overall accuracies could be improved by adding some orthogonal features to the original data. In the case of the present study, the texture features played a role of the orthogonal features and made the selected signatures of classes more separable in a multidimensional feature space.

Table 10. The overall classification accuracy of the classified image

	Birch	Larch	Pine	Spruce	Cedar
Birch	214	352	1	0	0
Larch	9	5126	3	19	65
Pine	1	275	97	17	154
Spruce	0	116	2	581	130
Cedar	1	37	21	182	2184

Overall Accuracy = (8202/9587) 85.55%.

Table 11. The overall classification accuracy of the classified image

	Birch	Larch	Pine	Spruce	Cedar
Birch	223	197	0	0	0
Larch	2	5496	0	15	32
Pine	0	141	103	9	142
Spruce	0	68	1	582	151
Cedar	0	4	20	193	2208

Overall Accuracy = (8612/9587) 89.83%.

Classification Result Using Fuzzy Convolution

In some cases, to increase the reliability of the classification of the initially classified images, fuzzy convolutions of different sizes can be applied. The fuzzy convolution creates a thematic layer by calculating the total weighted inverse distance of all the classes in a determined window of pixels and assigning the central pixel the class with the largest total inverse distance summed over the entire set of fuzzy classification layers, i.e., classes with a very small distance value will remain unchanged while the classes with higher distance values might change to a neighboring value if there are a sufficient number of neighboring pixels with class values and small corresponding distance values [30].In this

study, a fuzzy convolution with a 3x3 size window has been applied to the classification result of the multiple bands.

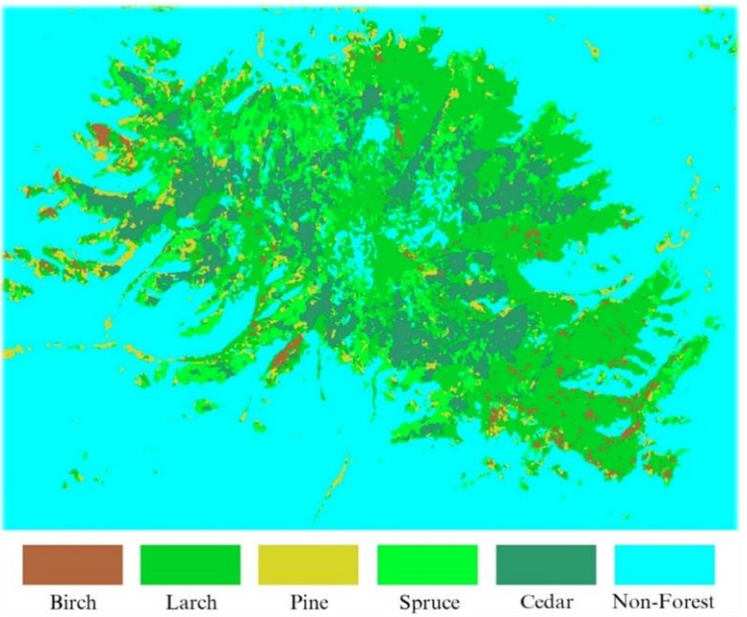

Figure 13. Classification result using fuzzy convolution.

The classified image is shown in Figure 13. The initial visual inspection of the fuzzy convolved image indicated that there are some improvements on the borders of the neighboring classes that influence the separation of the decision boundaries. The confusion matrix (Table 11) indicated an overall classification accuracy of89.83%. It is seen that the classification accuracy can be improved by the use of fuzzy convolution. As could be seen from the overall classification results, although the combined use of optical, SAR and texture features produced a better result, it is still very difficult to obtain a reliable forest map by the use of the standard technique.

The Refined Classification Method

For several decades, single-source multispectral data sets have been effectively used for forest mapping. Unlike single-source data, multisource data sets have proved to offer better potential for discriminating between different forest classes.

Generally, it is very important to design a suitable image processing procedure in order to successfully classify any RS data into a number of class labels. The effective use of different features derived from multiple sources and the selection of a reliable classification technique can be a key significance for the improvement of classification accuracy [43]. In this study, for the classification of forest classes, a refined MLC algorithm has been constructed. As the features, the multiple bands that include the original optical and SAR as well as three texture images have been used.

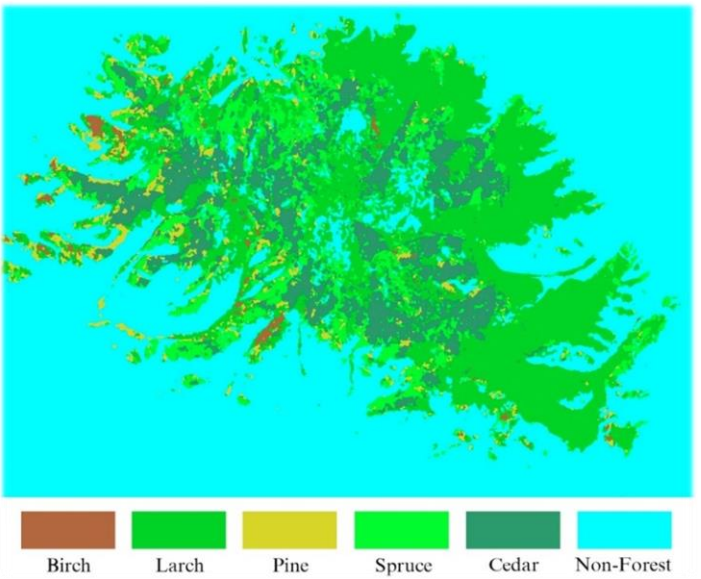

Figure 14. Classification result using the refined classification.

Unlike the traditional MLC, the constructed classification algorithm uses spatial thresholds defined from the contextual knowledge. The contextual knowledge is based on the spectral and textural variations of the available forest classes in different parts of the fused images and the thresholds are applied to separate the statistically overlapping classes. It is clear that a spectral classifier will be ineffective if applied to the statistically overlapping classes because they have very similar spectral characteristics. For such spectrally mixed classes, classification accuracies should be improved if the spatial properties of the classes of objects could be incorporated into the classification criteria. The idea of the spatial threshold is that it uses a polygon boundary to separate the overlapping classes and only the pixels falling within the threshold boundary are used for the classification.

In that case, the likelihood of the pixels to be correctly classified will significantly increase, because the pixels belonging to the class that overlaps with the class to be classified using the threshold boundary are temporarily excluded from the decision making process. In such a way, the image can be classified several times using different threshold boundaries and the results can be merged [44].

Table 12. The overall classification accuracy of the classified image

	Birch	Larch	Pine	Spruce	Cedar
Birch	223	95	0	0	0
Larch	2	5703	0	8	17
Pine	0	71	113	4	95
Spruce	0	33	0	689	80
Cedar	0	4	11	98	2341

Overall Accuracy =(9069/9587) 94.59%.

The result of the classification using the refined method is shown in Figure 14. For the accuracy assessment of the classification result, the overall performance has been used, taking the same number of sample points as in the multiple bands. The confusion matrix produced for the refined classification showed an overall accuracy of94.59% (Table 12). As could be seen from Figure 14, the result of the classification using the refined MLC method is better than the result of the standard method. A general diagram of the refined classification technique is shown is Figure 15.

Update of Forest GIS

GIS is a computer-based system capable of capturing, storing, analyzing, and displaying geographically referenced information – the information attached to a location [45]. The most commonly used method of data capturing is the digitization, where hard copy maps or survey plans are transferred into digital formats through the use of special software programs and spatial-referencing capabilities. With the emergence of modern ortho-rectified images acquired from both space and air platforms, heads-up digitizing is becoming the main approach through which positional data are extracted [46]. Compared to the traditional method of tracing, heads-up digitizing involves the tracing of spatial data directly on top of the acquired imagery. Thus, due to rapid development in science and

technology, primary spatial data acquisition within a GIS is becoming more and more sophisticated.

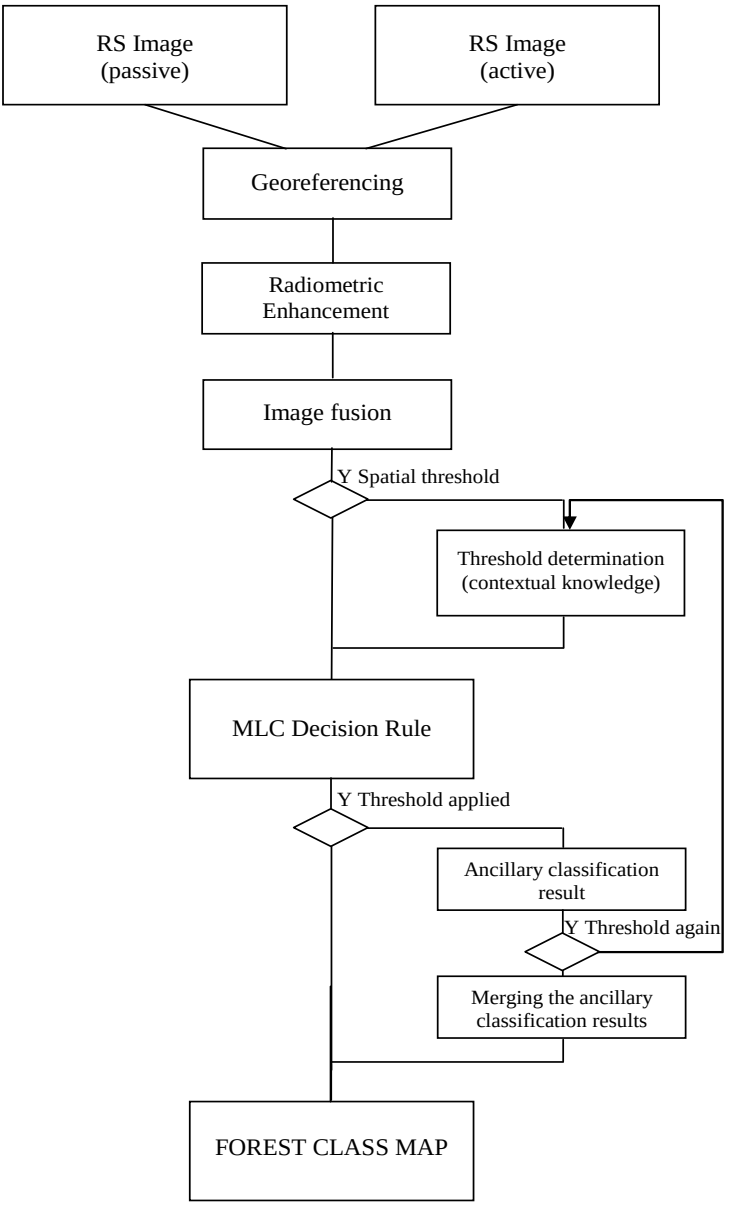

Figure 15. A general diagram for the refined classification.

(Table 10) 352 and 154 pixels of the same forest classes were misclassified as the birch and pine forests. Likewise, 489 pixels of the larch forest of the classified PC image have been misclassified as pine forest, whereas 275 pixels of the same class were classified as the pine forest.

As seen from the comparison of the classified images, the overall accuracies could be improved by adding some orthogonal features to the original data. In the case of the present study, the texture features played a role of the orthogonal features and made the selected signatures of classes more separable in a multidimensional feature space.

Table 10. The overall classification accuracy of the classified image

	Birch	Larch	Pine	Spruce	Cedar
Birch	214	352	1	0	0
Larch	9	5126	3	19	65
Pine	1	275	97	17	154
Spruce	0	116	2	581	130
Cedar	1	37	21	182	2184

Overall Accuracy = (8202/9587) 85.55%.

Table 11. The overall classification accuracy of the classified image

	Birch	Larch	Pine	Spruce	Cedar
Birch	223	197	0	0	0
Larch	2	5496	0	15	32
Pine	0	141	103	9	142
Spruce	0	68	1	582	151
Cedar	0	4	20	193	2208

Overall Accuracy = (8612/9587) 89.83%.

Classification Result Using Fuzzy Convolution

In some cases, to increase the reliability of the classification of the initially classified images, fuzzy convolutions of different sizes can be applied. The fuzzy convolution creates a thematic layer by calculating the total weighted inverse distance of all the classes in a determined window of pixels and assigning the central pixel the class with the largest total inverse distance summed over the entire set of fuzzy classification layers, i.e., classes with a very small distance value will remain unchanged while the classes with higher distance values might change to a neighboring value if there are a sufficient number of neighboring pixels with class values and small corresponding distance values [30]. In this

analysis. Over the past few years, RS techniques and technologies, including system capabilities have been significantly improved. Meanwhile, the costs for the primary RS data sets have drastically decreased [48]. This means that it is possible to extract from RS images different types of forest related information in a cost-effective way and update layers within a GIS.

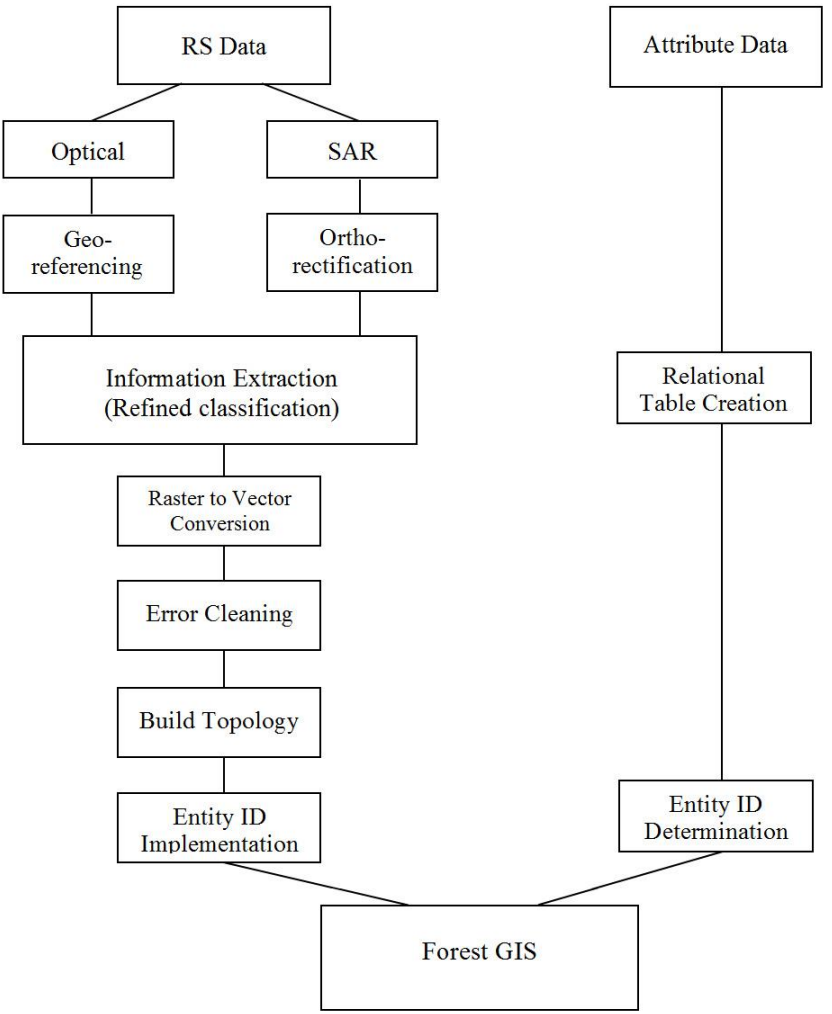

Figure 17. A diagram for update of forest GIS via processing of multisource RS images.

In the present study, it was assumed that there is an operational forest GIS that stores historical thematic layers and there was a need to update a forest class layer. The forest inventory data for the Bogdkhan Mountain was last updated in 1988. Therefore, the current layer was created using an existing forest taxonomy map of 1988 and the ArcGIS system was used for its digitizing. The digitized map is shown in Figure 16. As the overall classification accuracy of the classified multisource images exceeds 90%, the result can be directly used to update the layer of the operational GIS. For this end, a raster thematic map (i.e., classified image) extracted from the multisource RS data sets should be converted to a vector structure. After error cleaning and editing, the converted from raster to vector layer can be topologically structured and stored within the forest GIS. If one compares the forest layers created from the forest taxonomy map and classified RS image, could see what changes had occurred. A diagram for the update of a forest class layer of a GIS via processing of multisource RS images is shown in Figure 17.

Conclusion

The overall aimof this chapter was to evaluate the performances of different image fusion techniques for the enhancement of spectral and textural variations of different forest typesto be used for the training site selection and apply arefined classification method for the extraction of forest class informationfrom the multisource images in order to update a forest GIS. For the test area, Bogdkhan Mountain situated in the central part of Mongolia and one of the world’s oldest and officially protected sites, was selected.As the fusion techniques,modified IHS transformation, PCA technique, Gram-Schmidt method, color normalization spectral sharpening, wavelet-based fusion, and Ehlers method were used. Of these methods, the modifiedIHS transformation, PCA, and wavelet-based fusion gave better results compared to the other fusion techniques in terms of the spatial and spectral separations among different forest types. For the classification of the multisource images, the statistical MLC and refined method were used and the results were compared. In order to evaluate the classification accuracy of different features, the feature combinations were classified using the standard method. When the results were compared, the classification of the multiple bands, which included the original optical, SAR, and three texture images,gave the superior result. The constructed refined classification method used spatial thresholds defined from contextual knowledge and multiple features obtained through a feature derivation process. As could be seen from the classification results, the performance of the refined classification was much better than the performances

of the standard method and the output could be directly used to update forest GIS. Overall, the research indicated that multisource information can improve the interpretation and classification of forest classes and the elaborated refined classification method is a powerful tool in the production of a reliable forest map.

References

[1] Enkhjargal, D., Amarsaikhan, D., Battsengel, V. and Tsogzol, G. (2014). Applications of multitemporal optical images for forest resources study in Mongolia. In: *CD-ROM Proceedings of the ACRS*, Nay Pyi Taw, Myanmar, October 2014.

[2] Almeida, R., Shimabukuro, Y. E., Rosenqvist, A. and Sanchez, G. A. (2009). Using dual-polarized ALOS PALSAR data for detecting new fronts of deforestation in the Brazilian Amazonia. *International Journal of Remote Sensing*, Vol.30 (14), pp.3735-3743.

[3] Amarsaikhan, D., Battsengel, V., Amarjargal, Sh., Egshiglen, E., Ganzorig, M. and Enkhjargal, D. (2011). Applications of optical and microwave RS for forest mapping in Mongolia. In: *CD-ROM Proceedings of the ACRS*, Taipei, Taiwan, October 2011.

[4] Ferreira, L. G., Ferreira, N. C., Huete, A. R. and Ferreira, M. E. (2007). An operational deforestation mapping using MODIS data and spatial context analysis. *International Journal of Remote Sensing*, Vol. 28(1), pp.47-62.

[5] Badarinath, K. V. S., Sharma, A. R. and Kharol, S.K. (2011). *Forest fire monitoring and burnt area mapping using satellite data: a study over the forest region of Kerala State, India.* Vol. 32(1), pp.85-102.

[6] Matricardi, E. A. T., Skole, D. L., Pedlowski, M. A. and Chomentowski. (2013). *Assessment of forest disturbances by selective logging and forest fires in the Brazilian Amazon using Landsat data*. Vol. 34(4), pp.1057-1086.

[7] Todd, A., Schroeder, T. A., Healey, S. P., Moisen, G. G., Frescino, T. S., Cohen, W. B., Huang, Ch., Kennedy, R. E. and Yan, Zh. (2014).Improving estimates of forest disturbance by combating observations from Landsat time series with US Forest Service Forest Inventory and Analysis data. *Remote Sensing of Environment*, Vol.154, pp.61-73.

[8] Amarsaikhan, D., Ganzorig, M., Batbayar, G., Narangerel, D. and Tumentsetseg, Sh. (2004). An integrated approach of optical and SAR images for forest change study. *Asian Journal of Geoinformatics*, Vol. 4(3), pp. 27-33.

[9] Huang, Sh., Crabtree, R. L., Potter, Ch. and Gross, P. (2009).Estimating the quantity and quality of coarse woody debris in Yellowstone post-fire forest ecosystem from fusion of SAR and optical data. *Remote Sensing of Environment*, Vol. 113(9), pp.1926-1938.

[10] Morel, A. C., Fisher, J. B. and Malhi, Y. (2012). *Evaluating the potential to monitor aboveground biomass in forest and oil palm in Sabah, Malaysia, for 2000-2008 with Landsat ETM+ and ALOS-PALSAR.* Vol. 33(11), pp. 3614-3639.

[11] Hoan, N. T., Tateishi, R., Alsaaideh, B., Ngigi, T., Alimuddin, I. and Johnson, B. (2013). Tropical mapping using a combination and microwave data of ALOS. *International Journal of Remote Sensing,* Vol. 34(1), pp.139-153.

[12] Sybrand V. B., Comber, A. and Lamb, A. (2014).Random forest classification of salt marsh vegetation habitats using quad-polarimetric airborne SAR, elevation and optical RS data. *Remote Sensing of Environment*, Vol.149, pp. 118-129.

[13] Amarsaikhan, D., Saandar, M., Battsengel, V. and Amarjargal, Sh. (2012b). Forest resources study in Mongolia using advanced spatial technologies. *International Archives of the Photogrammetry, RS and Spatial Information Sciences, Vol. XXXIX-B7, XXII ISPRS Congress*, Melbourne, Australia.

[14] Amarsaikhan, D. and Douglas, T. (2004). Data fusion and multisource data classification. *International Journal of Remote Sensing*, No.17, Vol. 25, pp.3529-3539.

[15] Zhang, J. (2010), Multi-source remote sensing data fusion: status and trends. *International Journal of Image and Data Fusion*, 1, pp.5 – 24.

[16] Sritarapipat, T., Kasetkasem, T. and Rakwatin, P. (2014). Fusion and registration of THEOS multispectral and panchromatic images. *International Journal of Remote Sensing*, Vol. 35(13), pp.5120-5147.

[17] Karathanassi, V., Kolokousis, P. and Ioannidou, S. (2007).A comparison study on fusion methods using evaluation indicators. *International Journal of Remote Sensing*, Vol. 28, pp.2309 – 2341.

[18] Ehlers, M., Klonus, S. and Åstrand, P. J. (2008).Quality Assessment for multi-sensor multi-date image fusion, CD-ROM *Proceedings of ISPRS Congresses*, Beijing, China, July 3- 11, 2008.

[19] Fang, F., Li, F., Zhang, G. and Shen, C. (2013). A variational method for multisource remote-sensing image fusion. *International Journal of Remote Sensing*, Vol. 34(7), pp.2470–2486.

[20] Amarsaikhan, D. (2013). Environmental studies of Mongolia using RS and GIS techniques. *Proceedings of the International Conference* on Climate Changein Arid and Semi-Arid Region, Ulaanbaatar, Mongolia, pp.18-26.

[21] Kuplich, T.M., Freitas, C.C. and Soares, J.V. (2000).The study of ERS-1 SAR and Landsat TM synergism for land use classification. *International Journal of Remote Sensing,* Vol.21(10), pp. 2101-2111.

[22] Hyde, P., Dubayah, R., Walker, W., Blair, J. B., Hofton, M. and Hunsaker, C. (2006). Mapping forest structure for wildlife habitat analysis using multi-sensor (LiDAR, SAR/InSAR, ETM+, Quickbird) synergy. *Remote Sensing of Environment*, Vol. 102(1–2), pp.63-73.

[23] Cartus, O., Santoro, M., Schmullius, Ch. and Li, Z. (2011).Large area forest stem volume mapping in the boreal zone using synergy of ERS-1/2 tandem coherence and MODIS vegetation continuous fields. *Remote Sensing of Environment*, Vol. 115(3), pp.931-943.

[24] Dong, J., Xiao, X., Sheldon, S., Biradar, C., Duong, N. D.and Hazarika, M. (2012). A comparison of forest maps in Mainland Southeast Asia from multiple sources: PALSAR, MERIS, MODIS and ERA. *Remote Sensing of Environment*, Vol. 127, pp.60-73.

[25] Laurin, G. V., Liesenberg, V., Chen, Q., Guerriero, L., Frate, F. D., Bartolini, A., Coomes, D., Wilebore, B., Lindsell, J. and Valentini, R. (2013). Optical and SAR sensor synergies for forest and land cover mapping in a tropical site in West Africa. *International Journal of Applied Earth Observation and Geoinformation*, Vol.21, pp.7-16.

[26] Amarsaikhan, D., Ganzorig, M., Saandar, M., Blotevogel, H. H.,Egshiglen, E., Gantuya, R., Nergui, B. and Enkhjargal, D. (2012a).Comparison of multisource image fusion methods and land cover classification. *International Journal of Remote Sensing,* Vol. 33(8), pp.2532-2550.

[27] UNESCO. (1996). Mongolia Sacred Mountains: Bogd Khan, Burkhan Khaldun, Otgon Tenger, UNESCO World Heritage Center, available at http://whc.unesco.org/en/tentativelists/936.

[28] Amarsaikhan, D. and Sato, M. (2004).Validation of the Pi-SAR data for land cover mapping. *Journal of the Remote Sensing Society of Japan, No.2,* Vol. 24, pp.133-139.

[29] Serkan, M., Musaoglu, N., Kirkici, H. and Ormeci, C. (2008). Edge and fine detail preservation in SAR images through speckle reduction with an adaptive mean filter. *International Journal of Remote Sensing,* Vol. 29(23), pp. 6727 – 6738.

[30] ERDAS, (2010). New ERDAS Field Guide, *ERDAS*, Inc. Atlanta, Georgia, pp.776.

[31] ENVI, (2004). User's Guide, Research Systems Inc.

[32] Pohl, C. and Van Genderen, J. L. (1998). Multisensor image fusion in remote sensing: concepts, methods and applications. *International Journal of Remote Sensing*, Vol.19, 9, pp.823–854.

[33] Amarsaikhan, D., Bolorchuluun, Ch., Narangerel, Z. and Gantuya, R. (2009). Integration of RS and GIS for forest monitoring in Mongolia. In: *CD-ROM Proceedings of the Asian Conference on RS*, Beijing, China, October 2009.

[34] Jiang, D., Zhuang, D., Huang, Y. and Fu, J. (2011). Survey of multispectral image fusion techniques in remote sensing applications. *Image Fusion and Its Applications*, In Tech Open Access, pp.1-22.

[35] Siddiqui, Y. (2003).The modified IHS method for fusing satellite imagery. ASPRS 2003 *Annual Conference Proceedings*, American Society for Photogrammetry and Remote Sensing Anchorage, Alaska (CD publication).

[36] Richards, J. A. (2013). *Remote Sensing Digital Image* Analysis-An Introduction, ISBN-13: 978-3642300615, 5thEdition (Berlin: Springer-Verlag), pp.439.

[37] Laben, C. A., Bernard, V. and Brower, W. (2000). Process for enhancing the spatial resolution of multispectral imagery using pan-sharpening. United States Patent Application No. 6011875.

[38] Vrabel, J. C., Doraiswamy, P., McMurtrey, J. E. and Stern, A. (2002). Demonstration of the accuracy of improved resolution hyperspectral imagery. *Proceedings of SPIE 4725. Algorithms and Technologies for Multispectral, Hyperspectral, and Ultraspectral Imagery* VIII, pp.556–567.

[39] Pajares, G. and Cruz, J.M. (2004).A wavelet-based image fusion, *Pattern Recognition*. Vol. 37(9), pp.1855-1872.

[40] Klonus, S. And Ehlers, M. (2009). Performance of evaluation methods in image fusion, *Proceedings of 12th. International Conference on Information Fusion*, Seattle, USA, pp.1409-1416.

[41] Erbek, F. S., Zkan, C. O., Taberner, M. (2004).Comparison of maximum likelihood classification method with supervised artificial neural network algorithms for land use activities. *International Journal of Remote Sensing*, Vol. 25, pp.1733–1748.

[42] Mather, P. M. and Koch, M. (2010).*Computer Processing of Remotely-Sensed Images: An Introduction*, Fourth Edition, (Wiley, John & Sons).

[43] Lu, D. and Weng, Q. (2007).A survey of image classification methods and techniques for improving classification performance. *International Journal of Remote Sensing*, Vol. 28(5), pp.823-870.

[44] Amarsaikhan, D., Bat-Erdene, Ts., Ganzorig, M. and Nergui, B. (2013). Applications of remote sensing techniques and GIS for urban land change studies in Mongolia. *American Journal of GIS*, 2013. Vol. 2(3), pp.27-36.

[45] Folger, P. (2009).Geospatial information and geographic information systems: Current issues and future challenges. *Congressional Research Service*, CRS Report for Congress, pp.1-30.

[46] Amarsaikhan, D. and Ganzorig, M. (2010). *Principles of GIS for Natural Resources Management, 2nd edn* (Ulaanbaatar: Academic Press).

[47] Hwang, S. (2013).Placing GIS in sustainability education. *Journal of Geography in Higher Education*, Vol. 37(2), pp.276–291.

[48] Amarsaikhan, D. and Saandar, M. (2011).Chapter8 - Fusion of Multisource Images for Update of Urban GIS. *Image Fusion and Its Applications*, In TECH Open Access Publisher, pp.127-152.

Reviewed by Prof. Dr. J. Janzen, Free University of Berlin, Germany